



## FIELD-INDUCED TRANSPORT FOR INTERNAL AND INTERFACE SEGREGATION IN MULTIPHASE POLYMER FLOW SYSTEMS

\*M.B. KHAN

Nobel School of Chemical and Materials Engineering, NUST, Islamabad, Pakistan

The primary aim of this paper is to illustrate how certain processing variables influence the polymer structure and the extent of segregation in various flow geometries. A pronounced distinction is made between "diffusion" and "field-induced segregation". As opposed to diffusion in the classical sense, field-driven transport occurs *against* the concentration gradient. It is demonstrated that the application of an appropriate lateral field generates transversal migration of suspended material and, in certain cases, the segment domains in the "matrix" polymer. In particular, the potential of shear fields to generate locally segregated flow structures, which might be preserved during the fabrication procedure, has been assessed. Even though one finds a surprisingly large variety of driving forces available for lateral transport, the efficacy of highly specific processes resides in the novel application of boundary conditions. Convection-promoted shear transport has been investigated as a relevant example with an initial condition which specifies a cross-flow velocity component in an existing shear field. The investigation reveals that migratory transport in polymer processing channels has the potential to generate localized changes in the polymer morphology and structure, apart from affecting phase-redistribution of additive species on a more global scale. Experimental evidence on the phase-fractionation of poly-dispersed polyethylene and thermosetting polyurethane (PU) clearly demonstrates the phenomenon. The paper describes a new interface segregation system employing convection promoted field-induced transport for use in the thermoset reaction injection molding and other related polymer production processes. The proposed design mitigates the primary limitations of ordinary diffusion and other conventional external field migration system. The basic design concept is described and the key performance parameters are evaluated using established methods. An analytical model describes the time and space evaluation of the transverse concentration profile in the system and the results are compared with the experimental findings.

**Keywords :** Multiphase polymer flow, Internal segregation

### 1. Introduction

This paper deals with the phenomenon of diffusion and the external-field-induced migration that may be encountered in viscous multi-phase systems. A pronounced distinction is made between the terms "diffusion" and "field-induced migration". The former is conventionally regarded as the mass-transfer resulting from Brownian motion (random and spontaneous natural molecular movement) that occurs without the assistance of external forces. On the other hand, the latter usually implies that a suspended particle or macromolecule moves or drift, under the influence of external forces, relative to the carrier fluid velocity at its centre of mass, when its motion is observed over a period of time that is long compared to the time scale of the Brownian motion.

The principal practical application of diffusion and migration in this work concerns the production

of specific interface morphologies by segregation in a polyurethane (PU) reaction injection molding (RIM) and LDPE extrusion systems. The primary causes of segregation are the spatial variations in the diffusional driving forces. The diffusional flux is related to these mass-transfer driving forces. In Fickian or ordinary diffusion it is the gradient of concentration that provides the driving potential:

$$J = -D \partial C / \partial x \quad (1)$$

Where J is the flux, D is the diffusion coefficient, and x is the source coordinate in the direction of the diffusion.

As may be seen from (1), the segregation potential of Fickian diffusion is limited by a concentration gradient alone. In polymer fabrication processes such as RIM and extrusion, this is seldom capable of producing the required segregation during the time provided for diffusion or transport. This can be very simply seen by

\* Corresponding author : bilalkhan-ccems@nust.edu.pk

considering Einstein's expression for the mean distance  $d$  travelled by a solute molecule or particle in time  $t$  by concentration diffusion with diffusivity  $D$  [1]:

$$t = d^2 / 4D \quad (2)$$

For a typical RIM system where  $D = 10^{-13} \text{ m}^2/\text{s}$  and  $d = 0.001 \text{ m}$ , the time needed for diffusion works out to be  $\text{ca.}10^7\text{s}$ . This is almost infinitely long as compared to the time allowed for diffusion, which for moderately activated RIM system is around 60s. It is, therefore, normally necessary to augment the primary diffusion by convection (macroscopically observable flow) and/or by field-induced migration. The current paper will consider one such innovative application.

Another severe bottleneck which hinders the efficiency of all concentration transport processes is the lack of any mechanism for transporting the species *against* the concentration gradient. This becomes evident by examining the following thermodynamic relation for concentration transport:

$$\Delta G = RT \ln C_2 / C_1 \quad (3)$$

In which,  $\Delta G$  is the free energy change encountered in transporting the species from a concentration  $C_1$  to a concentration  $C_2$ .

The above equation indicates that the transport of species may be affected only when the free energy change associated with the transport process is negative or in other words if  $C_1 > C_2$ , in which case transport will occur spontaneously. Contrarily, if  $C_1 < C_2$ , the free energy change will either be zero or positive, under which conditions there will be no transport. It thus follows that the diffusion of species is not possible *against* the concentration gradient. However, transport against the concentration gradient may be performed by the application of external fields or forces which may also influence the rate of the transport process: the diffusion flux in the presence of external fields may then be expressed as:

$$J_T = J + J_F \quad (4)$$

Where  $J$  is the Fickian part of the total flux  $J_T$  and  $J_F$  is the flux due to the applied external field.

Typically, in a practical system, the external fields are applied at right angle to the direction of

the output flow. Several possible mechanisms may be used to augment the primary diffusion in the presence of an external field. These include: convection, pressure, thermal, electrostatic, electrophoresis, and stress-induced transport. To date most of these fields have found effective application in relatively low viscosity system (2-4). On the other hand, the significance of mass-transport in viscous systems such as the polymer production and processing sectors has been investigated only during the past decade or so [5-9]. A new interface segregation system that incorporates a unique combination of convection and stress-induced transport is described to demonstrate the viability of augmented transport in highly viscous systems such as PU RIM and extrusion.

## 2. The Model Field-Induced Segregation System

The model system considered here consists of two distinct external-field modules that are conveniently integrated into a singular flow geometry/configuration for achieving augmented transport of suspended matter in a viscous multiphase flow. The two modules, namely the shear stress module and the transverse injection module are combined in the drawing of Fig. 1.

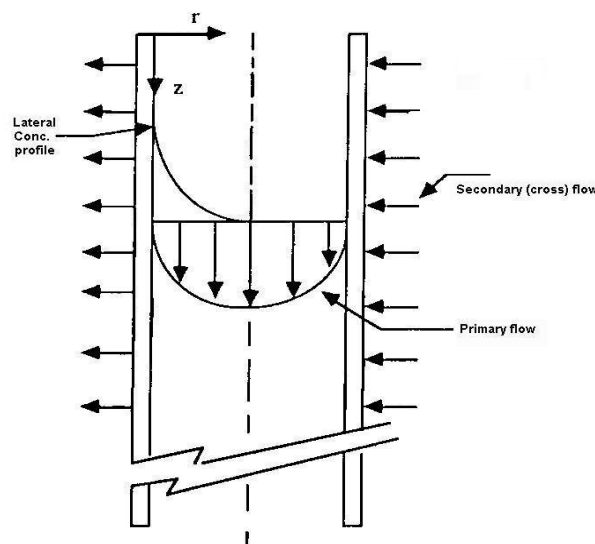


Figure 1. Lateral flow superposed on primary flow with the resultant concentration profile.

The shear stress module considers the shear stress difference across the suspended particle

due to the velocity gradient in the continuous phase contained in the Couette cell, Fig. 2. The rationale for this, of course, is that the drift velocity arises out of a pressure gradient in the non-homogeneous

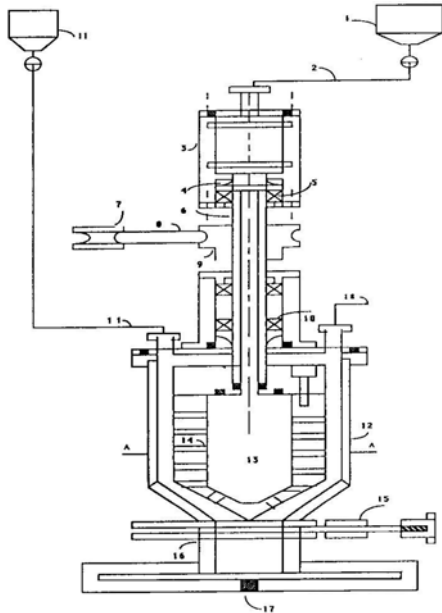


Figure 2. Couette cell incorporating radial flow.

flow. This may be seen from the following treatment of the Brenner's equation for the drift velocity experienced by a single isolated sphere when subjected to a velocity gradient in the carrier-fluid [10]:

$$V = d^2 (\text{Del}^2 U) / 6 \tag{5}$$

Where  $v$  is the drift velocity,  $d$  is the diameter of the 'particle' under migration, and  $u$  is the continuous-phase

velocity. Noting that in the Stokes flow, the Laplacian of the velocity field is related to the pressure gradient by:

$$U = \text{Del } p / \mu \tag{6}$$

Where  $\mu$  is the continuous-phase viscosity, it follows that the drift velocity may be interpreted as arising from a pressure gradient in the undisturbed Stokes flow. This pressure gradient is continuous through the Couette gap but acts *across* the dispersed phase particles as indicated in fig.3. As

a result the particles would tend to migrate through the shear gradient, seeking out regions of minimum shear or the outer stationary walls in the circular Couette flow system.

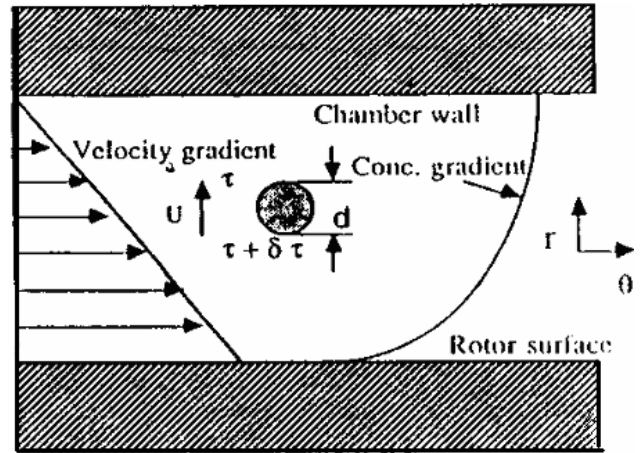


Figure 3. Schematic showing shear stress gradient across an isolated particle.

Two additional features need attention and must be secured. The provision of laminar flow and the optimization of the Couette gap in the cell. This is achieved by computing the cell  $Re$  to stay below about 3000. A more practical approach, however, is snapping the flow as a function of  $Re$  using a transparent cell made out of Perspex. Fig. 4 shows the results of such an experiment. Laminar to turbulent transition is clearly seen as one moves from a lower end high (800 rpm) to the turbulent limit (1500 rpm). Secondly, the Couette gap is optimized between the percent stress difference and the average shear rate operative for a given gap, as shown in Fig. 5.

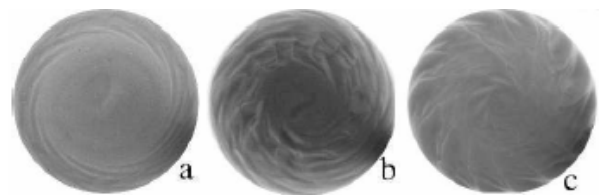


Figure 4. Laminar to turbulent transition with successive increment in the rotor rpm; for the present case a = 00 rpm, b = 1000 rpm, c = 1500 rpm.

Imparting an additional velocity component in the lateral or transverse direction further assists the potential of the shear-imposed migration. This is achieved by superimposing a macroscopic flow in the radial direction as depicted in Fig.1.

Innovatively a stream of the component to be segregated is injected radially through a porous inner wall. An extra flow (convective) component normal to the output flow is thus generated. The net result is a Couette device with a permeable rotor employing radial injection of the additive species for their facilitated transport to the bounding walls. The segregated structures generated thus may be preserved in the thermosetting PU polymer as it is discharged into a suitable cavity/mould. The characterization and assessment of the mould-part interface is then performed on the de-molded PU specimens using established methods as described in a subsequent section of this paper.

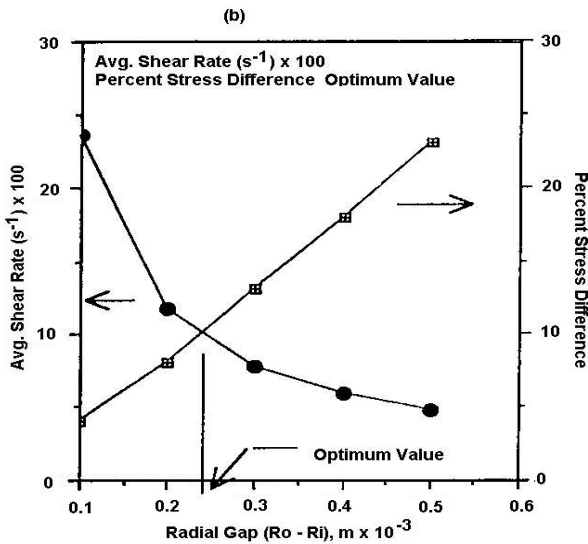


Figure 5. Optimization of the Couette annular gap.

2.1. Concentration distribution in the model system

The drift velocity and hence the particle flux is expressed in terms of net forces acting on the particles. The total flux of the particulate in the direction of the forces is then given by :

$$J_T = -D \partial C / \partial r + v(r). C \tag{7}$$

Where D is the ordinary self-diffusion coefficient of the particles, v(r) is the velocity of the particulate due to the applied lateral or external forces (negative by convention) and C is the local concentration of the particles. The particle velocity v (also termed as the drift velocity) may be expressed in terms of the convective, shear, and body forces operative in the annular gap of the

particle during its transport to the wall-polymer interface. Assuming Stokes law to apply, the particle velocity is expressed as :

$$V = (\delta \tau + V \Delta \rho \Omega^2 r) / 3 \pi \mu d + V_o \tag{8}$$

In which  $\delta \tau$  is the shear stress difference across the particle surface owing to the stress gradient in the annular gap, while the second term expresses the centripetal buoyancy of the particles. For neutrally buoyant particles this is zero.  $V_o$  is the initial radial velocity of the particles upon injection.

The first term in eqn. (7) above is too small to be included for solid particle transport in high polymer systems considered in this paper. The result is described by the dimensionless number  $d^2 / Dt$ , where d is the particle diameter, D its self-diffusion coefficient, and t is the time allowed for diffusion. When this number is of the order of unity or less, then the Brownian motion is effective [first term in eqn. (7)]. In the present work,  $d = 20 - 100 \mu m$ ,  $D = 10^{-13} m^2/s$ , and  $t = ca.60 s$ , implying that this number is much greater than unity and hence the first term may be conveniently neglected. Equation (7) thus reduces to:

$$J_T = -v(r). C \tag{9}$$

Differentiating w.r.t. the source coordinate, and noting that,  $\partial J_T / \partial r = \partial C / \partial t$ , one obtains:

$$\partial C / \partial t = \partial / \partial r (-v(r). C) \tag{10}$$

The species velocity V (given by eqn. 8) may be expressed in terms of the continuous-phase velocity u through the continuity relation:

$$u = -C.v / 1 - C \tag{11}$$

Where C is vol/vol concentration. u is commonly expressed in terms of the Couette parameters e.g. the radial frequency and the radial coordinate r. The final form of the concentration profile is then given in eqn.11 below, which is the corrected and modified solution form originally proposed by [11] in his work on transverse migration in various flow geometries of interest :

$$C(t,r) = (C_o/1-C_o) \exp-D' t/1 + (C_o/1-C_o) \exp-D' t/1 \tag{12}$$

In which  $D'$  is termed as the particle migration function and is expressed in terms of the system geometry and fluid properties :

$$D' = -k\Omega (R_o-r) (R_o-3r) / (R_o-R_i)^2 + 4D_o / R_i d \Omega (R_i^{-2} - R_i^{-2})^{-1} / R_o-R_i \quad (13)$$

Where  $d$  is the particle diameter,  $D$  is the injection hole diameter,  $R_i$  is the rotor radius,  $R_o$  is the cup radius,  $r$  is the radial coordinate and  $\Omega$  is the frequency of rotation. The factor  $k$  expresses the ratio of inertial and viscous effects for the situation of creeping flow:

$$K = \Delta \rho d^2 / 18 \quad (14)$$

With the correct value of  $D'$ , eqn. (12) describes the analytical concentration distribution for the model shear-injection system as a function of time ( $t$ ) and space ( $r$ ). The experimental profiles are presented and compared in a following section of this paper.

### 3. Intrinsic Field Transport

Perhaps the best example of an intrinsic field is the large negative enthalpy of the phase-separated state relative to the homogeneous mixture in the phase-separation process, commonly encountered in polymer blends and alloys. The phase separation in these amorphous, multi component systems is driven against the concentration gradient, starting from an initially homogeneous mixture. This process is quantified in terms of the Scott-Hildebrand solution theory [12, 13] and is expressed as a difference in the solubility parameters of the components and their molecular weights. The separation and/or phase redistribution of additives in polymers and composites is also largely attributed to this process as shown schematically in Fig. 6. Since the thrust of this paper resides in flow systems, it is not considered pertinent to dwell any further on the description of

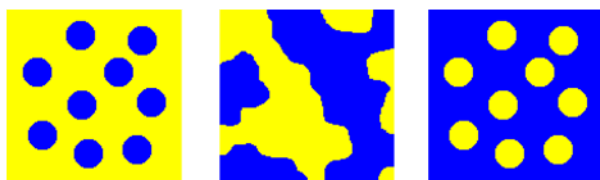


Figure 6. Phase segregation and inversion in polymer blend.

solid-phase segregation. The immediate discussion is directed toward the investigation of molecular migration in polydispersed polymer systems using model flow geometries.

#### 3.1. Macromolecular segregation

It has been suggested frequently that the presence of a stress field in a polymer system perturbs the average chain dimensions, elongating the chains in the direction of the flow. To counterbalance the situation, a thermodynamic force, entropic in origin, tends to restore the unperturbed dimensions of the macromolecule (the limitations of this hypothesis are discussed later). Reasonable speculation within the last few decades has proposed that this driving force will cause macromolecules to diffuse from regions of high stress to those of low stress, if such regions are present [14-17]. The force  $F$  is taken as the gradient of a potential field:

$$F = -\text{Del } V = u \cdot f \quad (15)$$

$V$  is the potential field, and  $u$  is the characteristic migration velocity as previously. For a flow field, the thermodynamic potential field is given as a function of the deformation rate [31]:

$$V = \kappa T [\tau^2 \gamma^2 / 3 - 1/2 \ln(1 + 2\tau^2 \gamma^2 / 3)] \quad (16)$$

In which  $\tau$  is the relaxation time of the polymer under migration, and  $\gamma$  is the deformation rate (shear rate) of the carrier fluid. Specification of  $\gamma$  as a function of the lateral or transversal position defines the potential field acting on a macromolecule, characterized by a relaxation time (typically for polymer solutions  $\tau$  is 0.01-0.10 s, and for polymer melts its values lies in the 1- 10-s range). So the opportunity of stress induced transport exists, whenever the deformation rate varies spatially. For tube flow :

$$\gamma = \frac{2u_o [1 - (r/R)]}{r} \quad (17)$$

whereas the appropriate expression for the deformation rate in circular Couette flow takes the form :

$$\gamma = \frac{2\Omega R_i^2 R_o^2}{[R_o^2 - R_i^2]}$$

Both the Couette and tubular flows represent non-homogeneous fields and are common processing geometries in most polymer operations e.g. the rotary screw extrusion and the on-line after-mixer assemblies encountered in the thermoplastic and thermoset reaction molding processes, respectively. Fig. 7 is a depiction of how secondary phase macromolecules orient in the stretching flow caused by a shear field. This compares with the orientation obtained in a biaxial stress field with the attendant analysis, Fig. 8. The latter is encountered in stretch blowing of PET bottles and the biaxial stretching of PET film in the draw and transverse directions. The stress in homogeneity in the latter cause the fine suspended particles to pop upto the surface to allow adhesion-free wind of the film on the spool [19].

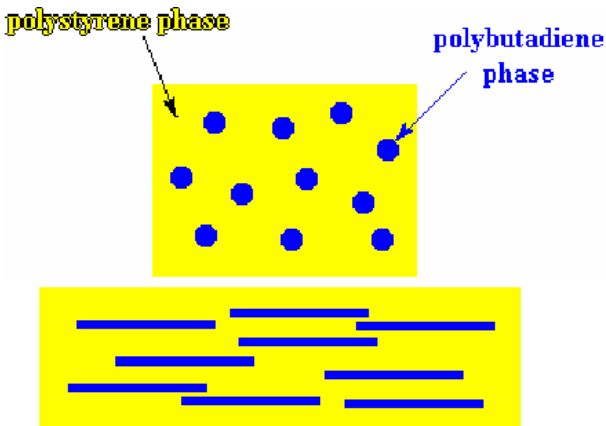


Figure 7. Elongation of secondary phase under unidirectional shear.

An alternative approach to macromolecular migration considers the macromolecule

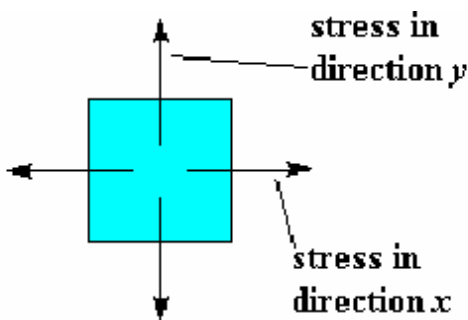


Figure 8. Biaxial stress shown for comparison.

as an elastic particle [18, 19]. Owing to the finite size of the chosen particle, a drift force is generated when it is subjected to a shear field, as shown in Fig. 9:

$$F = C_D L \sin \theta \cdot \dot{\gamma} \tag{19}$$

$C_D$  is the effective coefficient of resistance of A or B,  $L$  is the half-length of the particle, and  $\theta$  is the orientation angle of the particle. For  $\theta = 0$ , the particle lies along the streamline, and hence the lift force is zero, implying zero migration. The stored elastic energy for an ensemble of elastic particles is expressed as a function of shear rate and the carrier fluid viscosity :

$$U \propto (\dot{\gamma})^{4/3} (\mu)^2 \tag{20}$$

Since the deformation rate varies across the domain of the mixture, the elastic stored energy also varies along the same coordinate. The resultant forces would, therefore, tend to concentrate the macromolecules in regions of low stress field. The characteristic velocity for this migration may be computed by inserting the expression for the elastic potential field and solving Eq. (11). For the case of large interaction between the macromolecular segments, the following result was obtained [20,21]:

$$Y = 0.0085 \mu L^5 / kT (\dot{\gamma}^2 r) \tag{21}$$

where the numerical factor arises from the analytical integration.

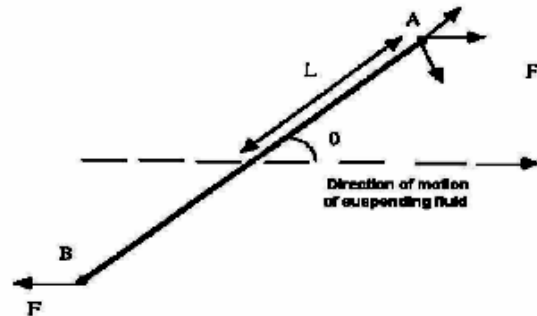


Figure 9. Coordinates of an isolated particle in shear field.

Experiments on the tube flow of viscoelastic polymer solutions and extrusion of multiphase and polydispersed polymer systems demonstrate that the observed degree of molecular migration is sensitive to the radius of the tube and the flow velocity, once the type of macromolecular fluid and the system temperature are specified (in this manner  $\tau$  and  $D$  are fixed) [22-24]. Both decreasing  $R$  and increasing  $u$  increase the effectiveness of the stress-induced transport. This should be expected as either of these increases

the shear rate (Eq. 13) and hence the intensity of the potential field (Eq. 12). It has also been observed that decreasing  $R$  is more effective than increasing  $u$  in producing this effect. Furthermore, the extent of the migration has been observed to be dependent on the  $L/R$  ratio of the tube; a ratio of normally greater than 100 is required to achieve any appreciable phase redistribution. Die Swell data in fig.10 on polydispersed LLDPE following extrusion through long capillaries indicate that there is phase redistribution on a more global scale as the higher molecular weight fraction is transported toward the center of the flow channel owing to the higher shear stress at the tube wall. This reduces the die swell and is more effective at higher shear rate.

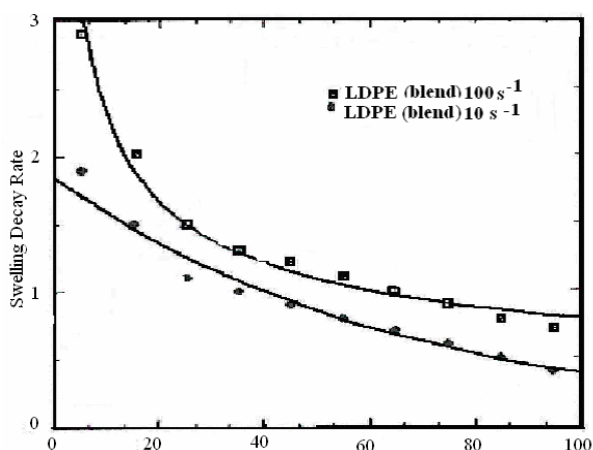


Figure 10. Swelling decay ratio vs. tube  $L/d$  for LDPE extrusion with shear rate as the parameter.

## 4. Experimental Materials and Methods

### 4.1 Materials

A polyester PU system supplied by 'B&T Polymers (U.K) was employed in this study. The resin exhibited a gel point of ca. 5 minutes at an average shear rate of  $250 \text{ s}^{-1}$  at  $30^\circ\text{C}$ .

Both liquid and solid injection systems were studied. The liquid additive supplied by TH. Goldschmidt AG (FRG) was a polyether diol having a viscosity of  $500 \text{ mPa}\cdot\text{s}$  at  $20^\circ\text{C}$  (Voranol EP 1900). The solid additive consisted of 20 $\mu$  glass beads supplied by Dow-Corning (U.K.). These were used as a multiphase system in conjunction with an inert fluid carrier silicone (Tegotrenn L1-720-T), also supplied by TH. Goldschmidt AG (FRG).

### 4.2 Injection – RIM

RIM experiments were performed by injecting the additive at a pre-determined rate through the porous rotor into the PU reaction mass contained in the annular space of the shear cell. The contents of the cell were then immediately discharged into an edge-gated disc mould to complete the polymerization at  $60^\circ\text{C}$ . The solid PU polymer was finally de-molded and subjected to surface and bulk characterization procedures. The additive injection rate and rotor RPM were employed as the major variables in this study. The former determined the injection velocity, while the later represented the stress differential operative in the Couette gap [25].

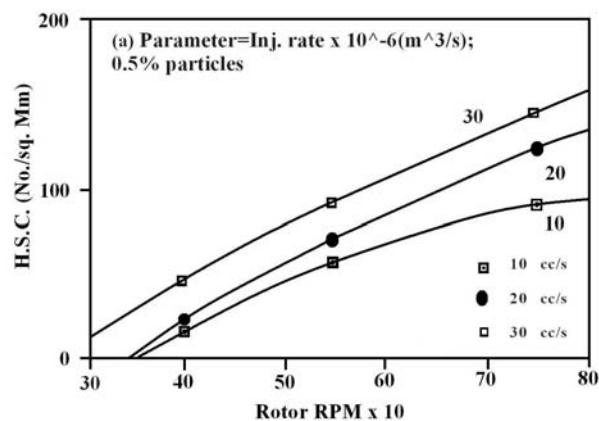


Figure 11. High spot count as function of rotor RPM with injection rate as parameter

### 4.3 Spatial characterization

The mean surface roughness,  $R_a$ , and the High Spot Count (HSC) of the fabricated polymer surfaces were measured to assess the particle protrusion and population in the surface regions, respectively. A stylus profilometer was used to perform these measurements.

### 4.4 HPLC

High Pressure Liquid Chromatography (HPLC) determined the concentration distribution of the liquid additives in the PU molding. A Perkin Elmer liquid chromatograph equipped with an Lc-25RI detector system was employed. Known weights of the de-molded specimens,  $0.01 \text{ m}$  in diameter, were immersed in a suitable solvent (THF) and the eluant solution extracted with time was run on the HPLC column for quantification.

The interface position of the solvent phase in the depth of the molding, during the course of release, was determined by the position of the advancing front  $x$  ( $0 \geq x \leq h/2$ ), where  $h$  is the total depth of the molding (0.004 m). The amount of the additive eluted from the swollen Fig. 12. Average surface roughness as function of rotor RPM with injection rate as parameter region of the PU molding specimen of volume  $V$ , where  $V = A(h/2 - x)$  at any time  $t$  is then given by the following mass balance:

$$m = C_o A (h/2 - x) \quad (21)$$

Where  $A$  is the cross-sectional area of the molding specimen, and  $C_o$  is the initial concentration of the additive in the molding. The mass,  $m$ , of the liquid additive eluted is easily determined from the extraction during the course of the experiment, and hence the position  $x$  could be directly determined.

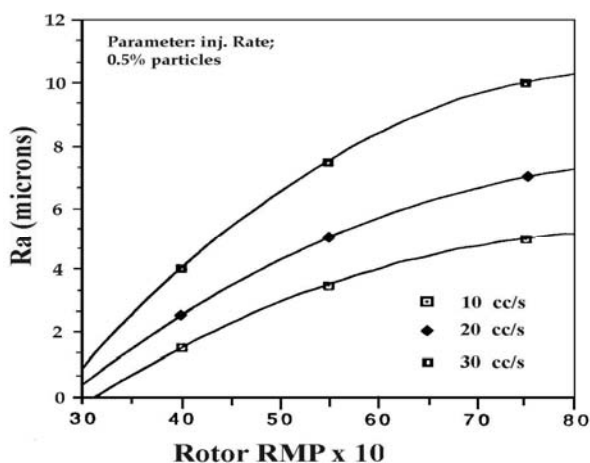


Figure 12. Average surface roughness as function of rotor RPM with injection rate as parameter.

## 5. Results and Discussion

### 5.1 Multiphase transport

This basically represents the solid particle transport and was primarily assessed by surface texture characterization of the RIM fabricated polymer specimens.

The surface roughness and HSC profiles of the particle-doped PU molding are shown in the Figures 11 and 12. HSC is a direct measure of the particle concentration. An increase in the average asperity height ( $R_a$ ) is noticed with increasing injection rate and RPM. The observed effect is

somewhat more pronounced for an increase in the injection rate. This should be expected since rotation accumulates the material towards the static wall (and hence the mould-part interface) owing to stress-induced transport. The radial injection, on the other hand, helps to transversely 'shoot' the particles through the stagnant layer at the stationary wall, thus overcoming the so-called skin effect.

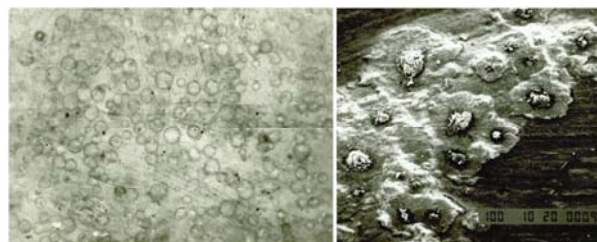


Fig. 13 (a) Molding fabricated by conventional mixing and casting showing skin effect without particle protrusion at surface (b) molding fabricated by field-induced transport.

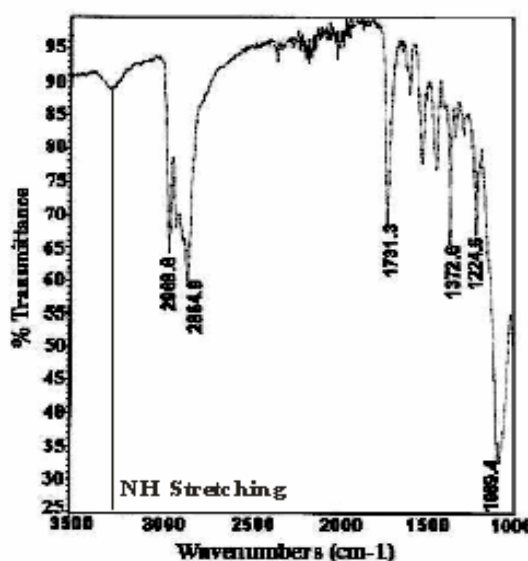


Figure 14. ATR-IR of the cross-linked PU specimen.

A comparison of the surface morphology of the recovered molding affords a direct manifestation of augmented transport in external-field-induced migration, as depicted in Fig. 13. The particles just lay underneath the surface in the molding fabricated from normal mixing/casting procedures. Contrarily, particles are clearly seen to protrude the surface regions under the influence of radial transport. The corresponding ATR-IR scans in Fig. 14 and Fig.15 indicate that the spectroscopic

properties are also influenced on a more global scale, the specimen fabricated under stress gradient possessing a higher microphase segregation between the polymer segment domains as indicated by the higher -NH stretching peak compared to its conventional counterpart.

### 5.2. HPLC

The concentration distribution of the liquid additive in the final cured molding is presented in Fig. 16. These are plots of fractional concentration (normalized to total concentration) vs. the fractional distance (normalized to total distance from the specimen surface).

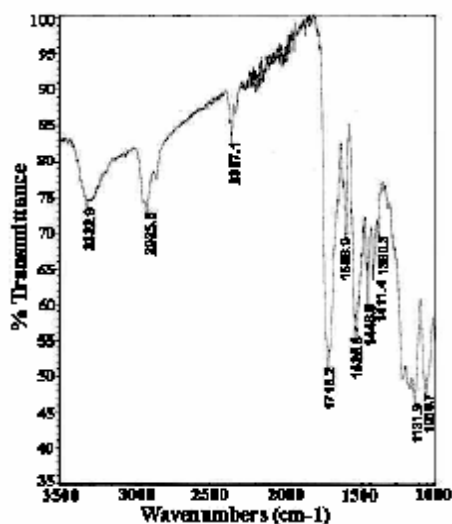


Figure 15. ATR-IR of the segmented PU specimen.

A quantitative comparison of the experimental and theoretical profiles is given in Figure 16. The theoretical curve is the one computed from eq. (12) for a time traverse of 10s. A cursory look at the two curves indicates that the steady-state profile is characterized by the total migration of the material to the interface, and that under the conditions of this experiment the time of traverse to reach equilibrium is ca.10 s. Further data on these systems for various operating times would presumably verify this assertion. Finally, the lower segregation values (higher concentration in the bulk of the moulding) for the experimental curve may have been promoted due to the entrainment of part of the injected fluid in the PU resin. This observation suggests the use of a separation efficiency factor for the external-field-induced segregation process.

In a recent study the geometry of interest consists of two concentric cylinders representing the walls of an extruder. The inner cylinder could be rotated to apply shear in the circumferential direction. Numerical simulations were performed on this geometry for conditions that are initially homogeneous (i.e., extrusion of a compositionally quenched blend) or phase separated (i.e., blend of two homopolymers).

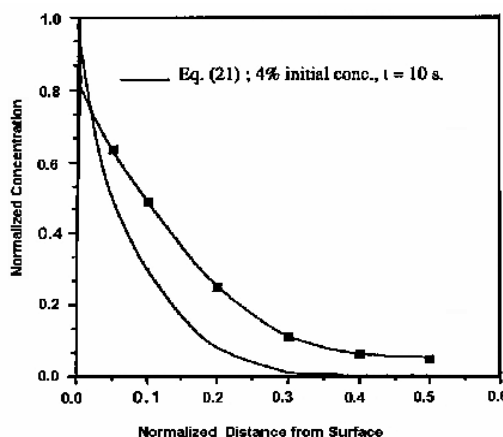


Figure 16. Comparison of the transversal concentration profiles.



Figure 17. Simulation of a two-phase extrusion showing alternating concentric regions of each phase. Shown is the morphology after 1 s (top) and 20 s (bottom).

Simulation results showed that including body force hastened phase ripening and that the resultant morphologies were similar to diffusion-only models. Applying shear had a tremendous effect on morphology. The appearance of phase boundaries was delayed, and there was a strong tangential orientation. This preferential orientation occurs because shear effects dominate at short and long times, whereas diffusion effects dominate

the intermediate stages. The final morphology appears as alternating concentric regions of each phase (Figure 17). The starting condition of the system seems to have little effect on the final morphology—thus the importance of spinodal decomposition in traditional melt blending and compositional quenching.

## 6. Conclusions

A new forced segregation system employing a novel combination of convective and shear fields has been described and its major performance features elucidated. In the light of the results obtained on the facilitated transport of the additive species, the current system may be described symbolically by the following descriptor:

$$D_s = G_1C_i + G_1V_1 + G_1V_2 + G_3V_3$$

Which states that the system is dominated by a concentration gradient in the  $x_1$  direction (radial direction), accompanied by a convective flow simultaneously, but in the  $x_1$ ,  $x_2$  (circumferential), and  $x_3$  (axial) direction, but which varies in strength in the  $x_1$  direction. This descriptor now provides a formal definition of the model system presented in this work. It has been shown that convection cum shear promoted transport is potent driving source for the accentuated migration of additive species in highly viscous systems. This provides one with the opportunity of fabricating specific mould-part interface morphologies in the PU RIM and other polymer processing sectors where mass transfer may influence the properties of the fabricated products.

It has been further shown that the concentration profiles obtained in the shear-injection process are generally exponential in nature, with the highest concentration at the mould-part interface and a thinning atmosphere of the additive extending through the rest of the space. The associated analytical study reveals that simple particle mechanical mass-transport models formulated using an effective drift velocity permit quantification of the exponential concentration profiles. Previously only rudimentary modeling had been performed. The current study, however, has been substantiated with advanced transport modeling capable of relatively accurate analytical prediction of the process.

The essential thesis of this paper is, however, that the process of convection assisted shear transport may have a significant and apparently predictable influence on the phase-segregation phenomenon encountered in high polymer multiphase systems. The current system may thus serve as a viable alternative to the more commonly found external fields, but which find their use only in low viscosity systems.

## References

- [1] J.L. Duda, *Pure and Appl. Chem.* **55** (1983) 861.
- [2] J.C. Giddings and M.N. Myers, *Analyt. Chem.* **46** (1974) 1917.
- [3] A. Stickler, *Sep. Sci. Tech.* **2** (1967) 235.
- [4] R.B. Bird, W.E. Stewart and E.N. Lightfoot "Transport Phenomena", Wiley, New York (1968).
- [5] B.D. Davis, *J. Appl. Polym. Sci.* **39** 1990) 2.
- [6] Chappleau and B.D. Favis, *J. Mat. Sci.* **30** (1995) 1.
- [7] M.B. Khan Energetic composites. Hand book of engineering polymeric materials. N.P. Ed. Cheremissinof, N.Y. Marcel Dekker (1997).
- [8] K. Min, J.L. White and J.F. Fellers, *Polym. Eng. Sci.* **24** (2004) 17.
- [9] D.P Quiroz, M.C. Concalves and N.P. Maria, *J. Appl. Polym. Sci.* **103** (2007) 1.
- [10] H. Brenner, *Chem. Eng. Sci.* **21** (1966) 97.
- [11] J. Harris Brit, *Soc. Rheol. Bull.* **15** (1972) 9.
- [12] R. L. Scott, *J. Chem. Phys.* **17** (1949) 279.
- [13] P. J. Flory. *Principle of Polymer Chemistry*, Cornell University Press, NY Ithaca (1953).
- [14] W. F. Busse, *J. Polym. Sci.* **A-2(5)** (1967) 1261.
- [15] A.P. Plochocky, *Adv. Polym. Technol.* **2** (2003) 4.
- [16] H.P Schreiber and S.H Storey, *Polym, J. Sci.* **B-3** (1965) 723.
- [17] A. B. Metzner, Y. Cohen and C. Ranyet-Nafail, *Non-Newtonian Fl. J. Mech* (1979) p. 5449.

- [18] J. H. Aubert and M. Tirrel, Chem. J. Phys. **72** (1980) 2694.
- [19] M. Tirrel and M.F. Malone, J. Sci. Polym., Ed. Phys. **15** (1977) 1569.
- [20] M.B. Khan and C. Keener, Polym Eng. Sci. **36**, (1996) 9.
- [21] E.B. Bagley, S.H. Storey and D. C West, J. Appl. Polym. Sci. **7** (1963) 1661.
- [22] J. Frenkel, Kinetic Theory of Liquids, Dover, New York (1955).
- [23] J. H. Aubert, S. Prager and M.Tirrel, J. Chem. Phys., **73**, (1980) 4103.
- [24] R. H. Shafer, Biophys. Chem. **2** (1974) 180.
- [25] M.B. Khan, B.J. Briscoe & S.M. Richardson, Polym. Eng. Sci. **30**, (1990) 175.